THE JOURNAL OF PHYSICAL CHEMISTRY B LETTERS

2005, *109,* 17350−17355
Published on Web 08/25/2005

Microwave Synthesis of Supported Au and Pd Nanoparticle Catalysts for CO Oxidation

Garry Glaspell, Lindsay Fuoco, and M. Samy El-Shall*

Department of Chemistry, Virginia Commonwealth University, Richmond, Virginia 21284-2006

Received: May 22, 2005; In Final Form: July 28, 2005

We report the microwave synthesis and characterization of Au and Pd nanoparticle catalysts supported on CeO_2, CuO, and ZnO nanoparticles for CO oxidation. The results indicate that supported Au/CeO_2 catalysts exhibit excellent activity for low-temperature CO oxidation. The Pd/CeO_2 catalyst shows a uniform dispersion of Pd nanoparticles with a narrow size distribution within the ceria support. A remarkable enhancement of the catalytic activity is observed and directly correlated with the change in the morphology of the supported catalyst and the efficient dispersion of the active metal on the support achieved by using capping agents during the microwave synthesis. The significance of the current method lies mainly in its simplicity, flexibility, and the control of the different factors that determine the activity of the nanoparticle catalysts.

Nanophase metal and metal oxide catalysts, with controlled particle size and shape, exhibit high surface area and densely populated unsaturated surface coordination sites that can result in significantly improved catalytic performance over conventional catalysts.[1−4] The large number of surface and edge atoms provide active sites for catalyzing surface reactions. Research in this area is motivated by the possibility of designing nanostructured catalysts that possess novel catalytic properties such as low-temperature activity, selectivity, stability, and resistance to poisoning and degradation effects.[1] Such catalysts are essential for technological advances in environmental protection, improving indoor air quality, and in chemical synthesis and processing.

Among the current important environmental issues is the low-temperature oxidation of carbon monoxide, since small exposure (ppm) to this odorless, invisible gas can be lethal.[5] Therefore, there is a need to develop highly active CO oxidation catalysts to remove even a small amount of CO from the local environment.

It has been demonstrated that nanoparticles of precious metals such as Au, Pd, and Pt, when used as CO oxidation catalysts, are not as susceptible to moisture and sulfur-containing compounds which typically affect the performance of transition metal oxide catalysts.[6,7] Haruta and co-workers demonstrated that the high surface area exhibited via Au nanoparticles makes them particularly useful for the catalytic oxidation of CO to CO_2.[8,9] The high activity of the Au catalysts is consistent with the strong tendency of Au nanoparticles to efficiently adsorb CO molecules. Surprisingly, the Au nanoparticles do not strongly adsorb and activate oxygen molecules.[10] Thus, it is now well-accepted that the oxide support plays a key factor in the activation of oxygen molecules during the CO oxidation.[11−13]

In this letter, we report a simple method to prepare Au and Pd nanoparticle catalysts supported on CeO_2, CuO, and ZnO and compare their catalytic activities for CO oxidation. We also demonstrate that the shape and morphology of the support nanoparticles can have a significant effect on the activity of the catalyst. The approach utilized in the present work is based on microwave synthesis of nanoparticles from metal salts in solutions. Microwave irradiation (MWI) has several advantages over conventional methods, including short reaction time, small particle size, narrow size distribution, and high purity.[14−18]

Synthesis of the nanoparticles of CeO_2, CuO, or ZnO was achieved by dissolving approximately 4 g of $Ce(NO_3)_4$, $Zn(NO_3)_2$, or $Cu(NO_3)_2$ (Alfa Aesar), respectively, in ethanol. While stirring, 10 N NaOH (Alfa Aesar) was added dropwise until the pH of the resulting solution was 10. The resulting solution was then placed in a conventional microwave. The microwave power was set to 33% of 650 W and operated in 30-s cycles (on for 10 s, off for 20 s) for 10 min. The resulting powder was washed with distilled water and ethanol and left to dry. M-doped oxide support nanoparticles (M = Au or Pd) were prepared as above, but with the addition of the appropriate amounts of the metal salt ($HAuCl_4$ or $Pd(NO_3)_2$) mixed with the $Ce(NO_3)_4$, $Zn(NO_3)_2$, or $Cu(NO_3)_2$ solution to obtain the desired dopant concentration (2%, 5%, or 10%). For capped nanoparticles, the starting precursors were mixed with poly(ethylene glycol) (PEG, molecular weight = 1450) or poly(*N*-vinyl-2-pyrrolidone) (PVP, molecular weight = 40 000) as a protective polymer prior to microwaving.

The X-ray diffraction (XRD) patterns of the powder samples were measured at room temperature with an X'Pert Philips Materials Research Diffractometer, with CuKα radiation. The samples were mounted on a silicon plate for X-ray measurements. For the CO catalytic oxidation, the sample was placed inside a Thermolyne 2100 programmable tube furnace reactor. The sample temperature was measured by a thermocouple placed near the sample. In a typical experiment, 4 wt % CO and 20 wt % O_2 in He was passed over the sample while the temperature was ramped. The gas mixture was set to flow over the sample at a rate of 100 cm^3/min controlled via MKS digital flow meters. The conversion of CO to CO_2 was monitored using an infrared gas analyzer (ACS, Automated Custom Systems, Inc.). All the catalytic activities were measured (using 20 mg sample) after a heat treatment of the catalyst at 300 °C in the reactant gas mixture for 15 min in order to remove moisture and adsorbed

10.1021/jp0526849 CCC: $30.25

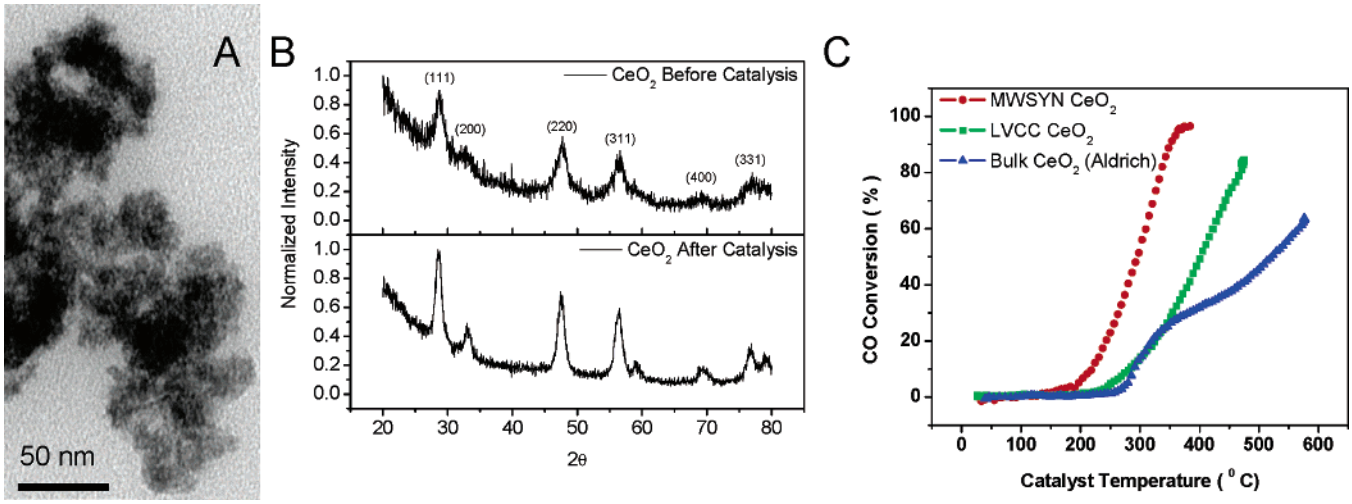

Figure 1. (A) TEM of CeO_2 nanoparticles prepared via microwave irradiation (the scale bar is 50 nm). (B) XRD of the CeO_2 nanoparticles as prepared (top) and after the oxidation of CO (bottom). (C) Temperature dependence for the CO conversion over: (blue) bulk CeO_2 (Aldrich, particle size <5 μm); (green) CeO_2 nanoparticles prepared by laser vaporization, particle size $\sim$20 nm; and (red) CeO_2 nanoparticles prepared by microwave irradiation, particle size $\sim$ 5 nm.

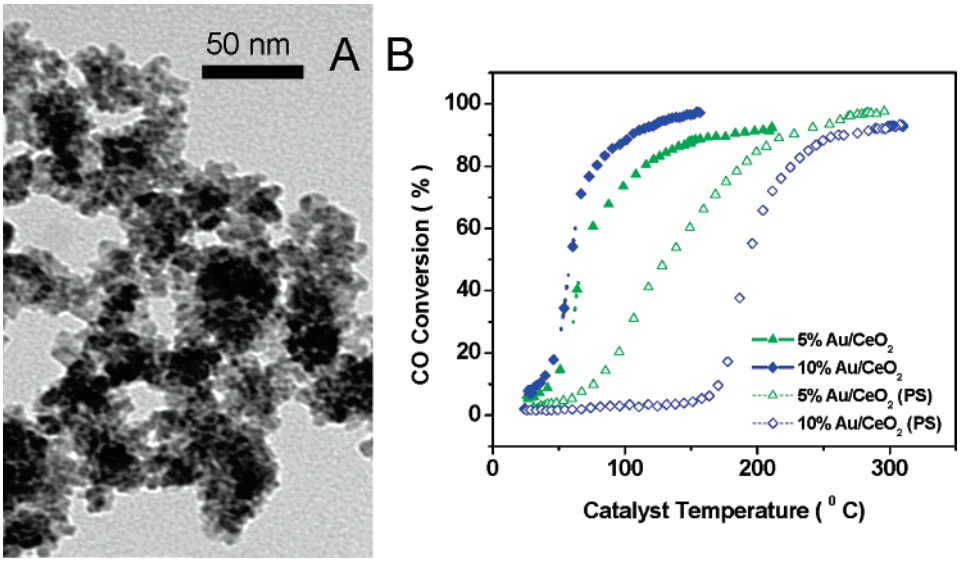

Figure 2. (A) TEM of 10% Au/CeO_2 nanoparticles. The scale bar is 50 nm. (B) Temperature dependence for the CO conversion over 2% and 10% Au/CeO_2 coprecipitated and precipitated separately (PS).

impurities. Transmission electron microscopy (TEM) was carried out using a Joel JEM-1230 electron microscope operated at 120 kV.

Figure 1A displays a typical TEM image for CeO_2 nanoparticles prepared via MWI. The individual particles have spherical shapes with average diameters of 4−5 nm with a significant degree of aggregation. The XRD pattern of the as-prepared nanoparticles, shown in Figure 1B (top), matches well with CeO_2 (ICCD 00-034-0394) from the database with no evidence of impurity peaks. Volume-weighted average crystalline size calculated from the XRD peak width using Scherrer's equation indicates that the average particle size of the ceria nanoparticles is smaller than 5 nm.[19]

Figure 1C compares the catalytic activities of the ceria nanoparticles prepared in our laboratory by MWI and by the Laser Vaporization-Controlled Condensation (LVCC) method[20] with the commercial ceria powder consisting of micron-size particles (Aldrich, <5 μm). The CeO_2 nanoparticles prepared by MWI exhibit 50% and 97% conversions of CO to CO_2 at temperatures of 295 and 387 °C, respectively. For comparison, a commercial ceria powder (Aldrich) with a specific surface area of 79 m^2 g^{-1} exhibits a 100% CO conversion at 450 °C.[21] The higher catalytic activity of the sample prepared by MWI is attributed to the small size of the nanoparticles. After the CO oxidation reaction, the XRD still shows the typical CeO_2 pattern without any indication of a phase change, as shown in Figure 1B (bottom). However, the average particle size after the catalysis test increases to $\sim$9 nm as determined via the peak widths in the XRD pattern. It is interesting to note that repeated catalysis tests after the first heat treatment result in reproducible CO conversion curves. This indicates that the advantages of the heat treatment resulting from removing moisture and generating clean surfaces outweigh the disadvantage of increasing particle size and subsequently decreasing surface area.

To examine the effect of the Au−ceria support interaction, we prepared 2%, 5%, and 10% Au/CeO_2. Figure 2A displays a representative TEM image of the Au/CeO_2 samples, specifically, the 10% Au/CeO_2 sample. The XRD patterns for 10% Au/CeO_2 before and after catalysis (Supporting Information) indicate that only CeO_2 peaks are present with no indication of Au diffraction peaks. This provides further support for the dispersion of the small Au nanoparticles within the ceria support.

TABLE 1: Temperatures for the Corresponding Conversions of CO over CeO_2, Au/CeO_2, and Pd/CeO_2 Nanoparticle Catalysts Synthesized by Microwave Irradiation

sample	$T_{3\%}$ (°C)	$T_{50\%}$ (°C)	% max (T °C)
CeO_2	170	295	97% (387)
2% Au/CeO_2	45	129	94% (245)
5% Au/CeO_2	<20	67	93% (211)
10% Au/CeO_2	<20	59	97% (156)
2% Au/CeO_2 (SP)[a]	120	239	94% (424)
5% Au/CeO_2 (SP)	36	132	98% (301)
10% Au/CeO_2 (SP)	49	172	91% (274)
2% Pd/CeO_2	137	190	100% (206)
5% Pd/CeO_2	70	140	100% (151)
10% Pd/CeO_2	85	141	100% (173)

[a] (SP): Separately precipitated.

To force the gold nanoparticles onto the surface of the support, we modified the original synthesis procedure by precipitating the support with NaOH before the Au solution was added. The XRD patterns for the 10% sample (see Supporting Information) show that Au peaks are present before and after the catalysis reaction, indicating that the Au nanoparticles are concentrated on the surface of the ceria particles. Figure 2B compares the effect of the Au loading on the catalytic activity of the coprecipitated and separately precipitated (SP) samples containing 5% and 10% Au, and the overall results for the catalysts supported on ceria are presented in Table 1. Increasing the metal loading increases the catalytic activity as a result of increasing the overlap between the metal and the support. However, in the coprecipitated catalysts, the 10% sample shows only slight improvement over the 5% sample, which may indicate that this is the maximum load that can be achieved with the MWI technique before the aggregation of the Au nanoparticles can significantly decrease the dispersion of the particles within the support. Interestingly, in the SP samples, the 5% Au is the most active sample, indicating that agglomeration of the Au nanoparticles to a larger size is more effective if the Au nanoparticles are present on the surface of the support. It is also clear that the coprecipitated catalysts exhibit significantly higher activities than the SP catalysts. For example, the best SP sample (5% Au) is still not as good as the worst coprecipitated sample (2% Au). This merely stresses the point that having Au nanoparticles uniformly dispersed within the oxide support is an important factor in determining the activity of the catalyst.

Figure 3 compares the CO conversions over 10% Au supported CeO_2, CuO, or ZnO nanoparticle catalysts prepared by the MWI method. It is clear that the ceria-supported catalyst exhibits the highest activity, and this is most likely due to the high oxygen storage capacity of ceria.[22] In this case, oxygen is assumed to adsorb on the ceria nanoparticles where it may or may not dissociate before reacting with CO molecules adsorbed on Au nanoparticles.[21,23] We also note that the activity of the 10% Au/CeO_2 catalyst prepared here by the MWI method is higher than that prepared by the coprecipitation method, but lower than similar catalysts prepared by deposition−precipitation (DP) and solvated metal atom dispersion methods.[21,24] This may suggest that the presence of small Au nanoparticles, as provided by the MWI method, is not the determining factor in achieving the highest CO conversion.[21] It appears that the presence of ionic gold well-dispersed within ceria, as provided by the DP method, is necessary to achieve the 100% room-temperature CO conversion.[21]

The TEM images of the Au/CuO and Au/ZnO catalysts, shown in Figure 3, reveal different morphologies from that observed in the Au/CeO_2 nanoparticle catalyst (Figure 2). Of

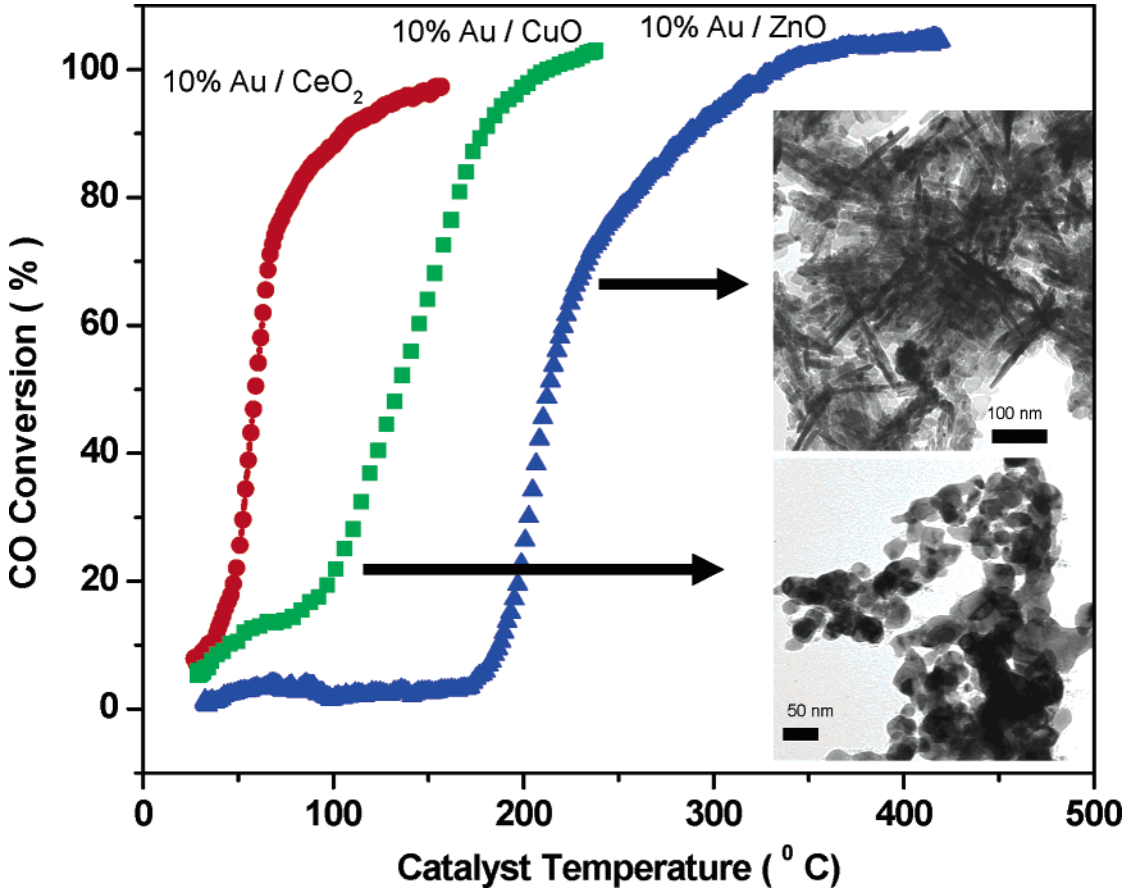

Figure 3. Temperature dependence for the CO conversion 10% Au/CeO_2, 10% Au/CuO, and 10% Au/ZnO.

TABLE 2: Temperatures for the Corresponding Conversions of CO over CuO, Au/CuO, and Pd/CuO Nanoparticle Catalysts Synthesized by Microwave Irradiation

sample	$T_{3\%}$ (°C)	$T_{50\%}$ (°C)	% max(T °C)
CuO	235	335	91% (550)
2% Au/CuO	130	177	97% (310)
5% Au/CuO	<20	112	100% (150)
10% Au/CuO	<20	135	100% (211)
2% Pd/CuO	94	160	98% (215)
5% Pd/CuO	75	131	98% (186)
10% Pd/CuO	63	124	97% (192)

TABLE 3: Temperatures for the Corresponding Conversions of CO over ZnO, Au/ZnO, and Pd/ZnO Nanoparticle Catalysts Synthesized by Microwave Irradiation

sample	$T_{3\%}$ (°C)	$T_{50\%}$ (°C)	% max(T °C)
ZnO	489		8% (535)
2% Au/ZnO	206	305	99% (420)
5% Au/ZnO	212	305	99% (418)
10% Au/ZnO	175	213	100% (331)
2% Pd/ZnO	177	210	99% (223)
5% Pd/ZnO	126	194	98% (200)
10% Pd/ZnO	162	189	99% (194)

special interest is the formation of long ZnO nanorods with lengths of several hundred nanometers and diameters of 10−15 nm in the Au/ZnO catalyst. It appears that the nanorod morphology does not allow for a uniform dispersion of the Au nanoparticles. This may explain the low activity of the Au/ZnO catalyst as indicated by the high temperatures needed to achieve high CO conversions. The CO conversion results over the catalysts supported on CuO and ZnO nanoparticles are presented in Tables 2 and 3, respectively.

Figure 4A displays a typical TEM image of the 10% Pd/CeO_2 nanoparticles. It is clear that the particles have a narrow size distribution with no evidence for agglomeration (the average particle diameter is 3−4 nm). XRD indicates that the Pd (similar to the Au) remains dispersed within the CeO_2 even after the catalysis reaction. The CO conversions over the 10% Pd catalyst supported on CeO_2, CuO, and ZnO nanoparticles are shown in Figure 4B, and the results for other catalysts with 2% and 5% Pd loadings are reported in Tables 1−3.

The small particle size and the narrow size distribution of the Pd/CeO_2 nanoparticles may be related to rapid nucleation followed by a slow growth process, which prevents particles from growing during the time scale of the MW irradiation. It is well-known that, when nucleation and growth can be separated, particles with a narrow size distribution are obtained.[25] Therefore, the current results also indicate that the nucleation and growth processes are very different in the Au/CeO_2 and Pd/CeO_2 systems. This could be related to the difference between interfacial free energies of the Au−CeO_2 and Pd−CeO_2 interfaces.

The high activities of the Au/CeO_2 and Pd/CeO_2 nanoparticle catalysts prepared by MWI are attributed to the strong interaction between Au or Pd and CeO_2 and to the oxygen storage capacity and redox properties of CeO_2 nanoparticles.[21−24] However, the low activity of the catalysts supported on the ZnO is attributed to the nanorod morphology, which appears to result in poor dispersion and aggregation of the metal nanoparticles. To stabilize the metal nanoparticles against agglomeration, the MW synthesis was carried out in the presence of PEG or PVP as a solvent for the starting materials. Figure 5A demonstrates that the MW-synthesized ceria nanoparticles in the presence of PVP have significantly smaller diameters and narrower size distribution than those prepared in the absence of PVP.

Figure 5B compares the CO conversions over the Au/ZnO catalyst prepared in the absence and presence of PVP. The TEM images displayed in Figure 5B clearly demonstrate the disappearance of the nanorod morphology of ZnO and the appearance of well-dispersed Au nanoparticles in the catalyst sample prepared in the presence of PVP. It is evident that PVP acts as a stabilizing agent for the growth of the Au nanoparticles and protects them from aggregation and increase in size. The enhanced catalytic activity of the Au/ZnO/PVP catalyst observed at lower temperatures is remarkable, since it directly correlates with the change in the catalyst morphology.

Similar effects are observed by using PEG as a capping agent during the MWI synthesis of the Pd/CeO_2 and Pd/ZnO catalysts as shown in the Figure 5C. Again, a significant increase in the CO conversion is observed for the Pd/CeO_2 catalyst prepared in the presence of PEG, as shown in Figure 5C (left). Also, a remarkable change in the morphology of the catalyst accompanied by enhanced activity is observed for the Pd/ZnO catalyst prepared in the presence of PEG, as shown in Figure 5C (right). The CO conversion results for the catalysts prepared in the presence of PVP or PEG are presented in Table 4.

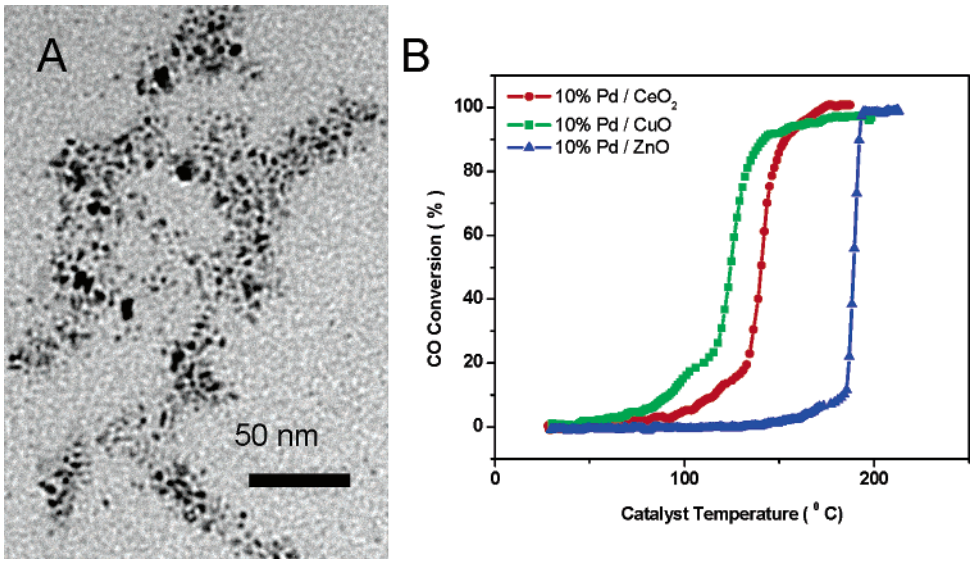

Figure 4. (A) TEM of 10% Pd/CeO_2 nanoparticles (the scale bar is 50 nm). (B) Temperature dependence for the CO conversion 10% Pd/CeO_2, 10% Pd/CuO, and 10% Pd/ZnO.

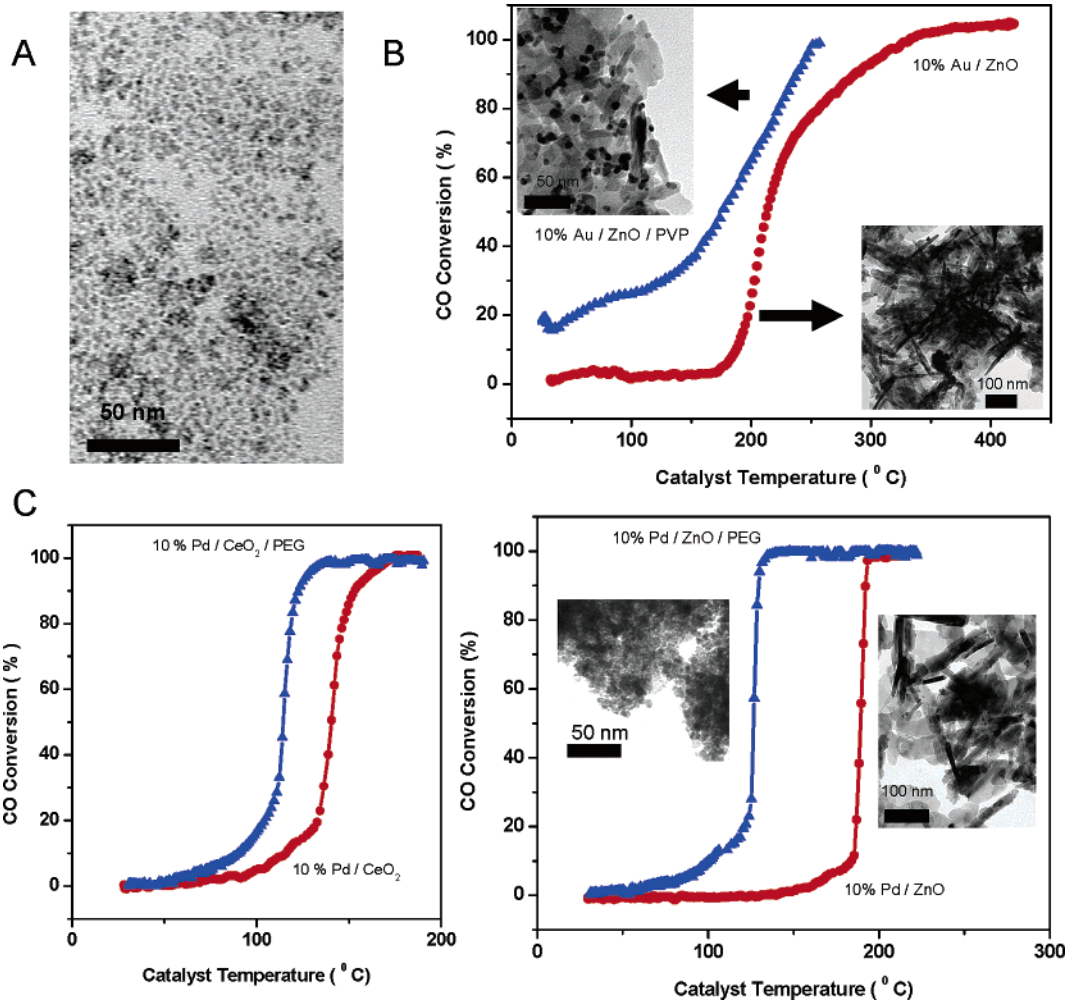

Figure 5. (A) TEM of CeO_2 nanoparticles prepared in the presence of PVP (the scale bar is 50 nm). (B) Comparison of CO conversion over 10% Au/ZnO catalyst prepared in the presence and absence of PVP. (C) (left) Comparison of CO conversion over 10% Pd/CeO_2 catalyst prepared in the presence and absence of PEG. (right) Comparison of CO conversion over 10% Pd/ZnO catalyst prepared in the presence and absence of PEG.

TABLE 4: Temperatures for the Corresponding Conversions of CO over Nanoparticle Catalysts Synthesized by Microwave Irradiation in the Presence of PVP or PEG

sample	$T_{3\%}$ (°C)	$T_{50\%}$ (°C)	% max(T °C)
CeO_2 (PVP)	215	332	99% (407)
CeO_2 (PEG)	175	309	99% (333)
ZnO (PVP)	241	333	99% (377)
ZnO (PEG)	227	308	98% (348)
10% Au/CeO_2 (PVP)	35	103	98% (267)
10% Au/CeO_2 (PEG)	<20	109	99% (353)
10% Au/ZnO (PVP)	<20	176	99% (252)
10% Au/ZnO (PEG)	132	324	99% (387)
10% Pd/CeO_2 (PVP)	134	179	98% (254)
10% Pd/CeO_2 (PEG)	62	114	99% (138)
10% Pd/ZnO (PVP)	172	219	99% (223)
10% Pd/ZnO (PEG)	68	127	99% (136)

Because of the high dielectric constant of PEG, it is an efficient absorber of MW radiation, and hence, rapid heating occurs easily under MW irradiation. In this case, the fast heating achieved by the presence of PEG accelerates the reduction of the metal precursor and leads to the formation of supersaturated metal solutions, which undergo rapid nucleation resulting in the formation of metal nanoparticles. The higher the supersaturation, the higher the nucleation rate and the smaller the critical sizes of the nuclei necessary to overcome the barrier to nucleation.[26] In addition, the rapid MW heating provides uniform temperature and concentration conditions for the nucleation and growth. Because of the strong dependence of nucleation rate on temperature and supersaturation, uniform heating results in a narrow particle size distribution, which increases the activity of the catalyst.

Finally, the high activity and stability of the nanoparticle catalysts prepared using the MWI method in the presence of capping agents method are remarkable and imply that a variety of efficient catalysts can be designed and tested using this approach. The significance of the current method lies mainly in its simplicity, flexibility, and the control of the different factors that determine the activity of the nanoparticle catalysts. The method allows the incorporation of one or more types of active metals such as Pd, Pt, Au, and Cu, or bimetallic alloys such CuAu, PdAu, and CuPd, as well as one or more type of oxide supports. We are currently exploring the effects of MW frequency, duration, and solvent polarity on the morphology, particle size, and size distribution of the nanoparticle catalysts.

In conclusion, a simple method has been developed for the synthesis of supported nanoparticle catalysts via microwave irradiation. This method offers extremely short reaction times and produces high purity and high yield of efficient nanoparticle catalysts.

Acknowledgment. Acknowledgment is made to the Donors of the American Chemical Society Petroleum Research Fund (PRF #41602-AEF) for financial support of this research.

Supporting Information Available: XRD data of the Au/CeO_2 nanoparticle catalysts before and after the CO catalysis test. This material is available free of charge via the Internet at http://pubs.acs.org.

References and Notes

(1) Moser, W. R., Ed. *Advanced Catalysts and Nanostructured Materials*; Academic Press: New York, 1996.

(2) Valden, M.; Lai, X.; Goodman, D. W. *Science* **1998**, *281*, 1647−1650.

(3) McCrea, K. R.; Parker, J. S.; Somorjai, G. A. *J. Phys. Chem. B* **2002**, *106*, 10854−10863.

(4) Ahmadi, I. S.; Wang, Z. L.; Green, T. C.; Henglein, A.; El-Sayed, M. A. *Science* **1996**, *272*, 1924.

(5) *Carbon Monoxide. Environmental Health Criteria*; World Health Organization: Geneva, 1999; p 213.

(6) Flytzani-Stephanopoulous, M. *MRS Bull*. **2001**, 885.

(7) Sinfelt, J. H.; Via, H.; Lythe, F. W. *J. Chem. Phys*. **1980**, *72*, 4832.

(8) Haruta, M. *Chem. Rec*. **2003**, *3*, 75.

(9) Haruta, M.; Tsubota, S.; Kobayashi, T.; Kageyama, H.; Genet, M. J.; Delmon, B. *J. Catal*. **1993**, *144*, 175.

(10) Liu, Z. P.; Hu, P.; Alavi, A. *J. Am. Chem. Soc*. **2002**, *124*, 14770.

(11) Haruta, M. *Catal. Today* **1997**, *36*, 153.

(12) Schubert, M. M.; Hackenberg, S.; van Veen, A. C.; Muhler, M.; Plazak, V.; Behm, R. J. *J. Catal*. **2001**, *197*, 113.

(13) Xu, Y.; Mavrikakis, M. *J. Phys. Chem. B* **2003**, *107*, 238.

(14) Kleinwechter, H.; Janzen, C.; Knipping, J.; Wiggers, H.; Roth, P. *J. Mater. Sci*. **2002**, *37*, 4349−4360.

(15) Zhu, J.; Palchik, O.; Chen, S.; Gedanken, A. *J. Phys. Chem. B* **2000**, *104*, 7344.

(16) Boxall, D.; Lukehart, C. *Chem. Mater*. **2001**, *13*, 806, 891.

(17) Gallis, K.; Landry C. *Adv. Mater*. **2001**, *13*(1), 23.

(18) Liang, J.; Deng, Z. X.; Jiang, X.; Li, F.; Li, Y. *Inorg. Chem*. **2002**, *41*, 3602.

(19) Klug, H. P.; Alexander, L. E. *X-ray Diffraction Procedures for Polycrystalline and Amorphous* Materilas, 2nd ed.; Wiley: New York, 1974.

(20) El-Shall, M. S.; Abdelsayed, V.; Pithawalla, Y. B.; Alsharach, E.; Deevi, S. C. *J. Phys. Chem. B* **2003**, *107*, 2882.

(21) Venezia, A. M.; Pantaleo, G.; Longo, A.; Di Carlo, G.; Casaletto, M. P.; Liotta, F. L.; Deganello, G. *J. Phys. Chem. B* **2005**, *109*, 2821.

(22) Travarelli, A.; Leitenburg, C.; Dolcetti, G.; Boaro, M. *Catal. Today* **1999**, *50*, 353.

(23) Frost, J. C. *Nature (London)* **1988**, *18*, 577.

(24) Stoeve, S. L.; Prasad, B. L. V.; Uma, S.; Stoimenov, P. K.; Zaikovski, V.; Sorensen, C. M.; Klabunde, K. A. J. *J. Phys. Chem. B* **2003**, *107*, 7441.

(25) Ramaswamy, V.; Haynes, T. E.; White, W.; Chan, W. J. M.; Roorda, S.; Aziz, M. J. *Nano Lett.* **2005**, *5*, 373−377.

(26) Kashchiev, D. *Nucleation: Basic Theory with Applications*; Butterworth Heinemann: Oxford, 2000.